# Exploration of ZnO Doped Nitrogen-Carbon Derived from Polyamide-Imide for Propane Dehydrogenation

Huahua Zhao , Tingyu Ji , Yanping Wu , Huanling Song , Jianfeng Wu * , Lingjun Chou *

Posted Date: 29 November 2023

doi: 10.20944/preprints202311.1776.v1

Keywords: Polyamide-imide; ZnO doped nitrogen-carbon; Propane dehydrogenation; Propene

*Article*

# Exploration of ZnO Doped Nitrogen-Carbon Derived from Polyamide-Imide for Propane Dehydrogenation

**Huahua Zhao [a], Tingyu Ji [b], Yanping Wu [c], Huanling Song [a], Jianfeng Wu [a, b,*] and Lingjun Chou [a,*]**

[a] State Key Laboratory for Oxo Synthesis and Selective Oxidation, Lanzhou Institute of Chemical Physics, Chinese Academy of Sciences, Lanzhou 730000, China

[b] State Key Laboratory of Applied Organic Chemistry, Key Laboratory of Special Function Materials and Structure Design (MOE), College of Chemistry and Chemical Engineering, Lanzhou University, Lanzhou 730000, P. R. China

[c] Key Laboratory of Science and Technology on Wear and Protection of Materials, Lanzhou Institute of Chemical Physics, Chinese Academy of Sciences, Lanzhou 730000, China

* Correspondence: authors: wjf@lzu.edu.cn; ljchou@licp.cas.cn

**Abstract:** A series of ZnO doped nitrogen-carbon materials (xZnO-N-C) with ZnO content of 5-40% are prepared by vacuum curing-carbonization strategy using polyamide-imide as N-C source and zinc nitrate as metal source for propane dehydrogenation (PDH). 20ZnO-N-C exhibits outstanding initial activity (propane conversion of 35.2% and propene yield of 24.6%) and relatively low deactivation rate (0.071 $h^{-1}$) at 600 °C. The detailed characterization results show that small ZnO nanoparticles (5.5 nm) with high dispersion on the catalyst could be obtained by adjusting ZnO loading. Moreover, much more nitrogen-based species especially $ZnN_x$ species are formed on 20ZnO-N-C by comparison with 20ZnO-N-C-air prepared by curing-carbonization without vacuum, which may contribute for the higher product selectivity and catalytic stability of 20ZnO-N-C. The probable active sites for PDH reaction on the catalyst system are proposed to be C=O species and $Zn^{2+}$ species. Moreover, the aggregation of ZnO nanoparticles is the primary reason for the activity loss on this catalyst system. The present finding not only provides the feasible construction strategy for the metal oxide doped nitrogen-carbon materials but also valuable guidance for the design of efficient catalyst in dehydrogenation of light alkane.

**Keywords:** polyamide-imide; ZnO doped nitrogen-carbon; propane dehydrogenation; propene

## 1. Introduction

The selective activation of inert but ubiquitous C-H bond in hydrocarbon molecules remains utmost importance and formidable challenge in catalysis and even in chemistry field [1, 2]. Light alkenes, such as propylene, as the key raw material and the primary product of petrochemical industry, have attracted ever-increasing attention [3]. Propylene is one of the basic feedstock for production of plastics, packaging materials and synthetic fibers in the global chemical industry. Therefore, on-purpose propylene production technology especially propane dehydrogenation (PDH) is of great interest to the petrochemical market in virtue that it is an important way to expand the source of propylene by non-petroleum cracking route [4].

Owing to the highly endothermic characteristic of PDH reaction, side reactions including propane cracking, deactivation by coke formation and metal sintering, easily occur under the required high temperature (550-600 °C), severely impeding the practical application [5]. Currently, nevertheless, PDH reaction has heavily depended on the utilization of the precious metals such as platinum and toxic transition metal oxides such as chromium oxide industrially [6]. Therefore, it is highly attractive to explore a low-cost and non-toxic catalyst material for PDH with industrial-level propylene selectivity and catalytic stability.

Tremendous alternative catalyst systems including metal oxides such as $VO_x$, $FeO_x$, ZnO et al., metal sulfides and carbon materials have been extensively developed and their design concepts could

 doi:10.20944/preprints202311.1776.v1



provide important reference for the development of efficient dehydrogenation catalyst [7-12]. Recently, exploration of Zn species as active component of dehydrogenation catalyst has extensively emerged in addition to the role as promoters [13-16]. In particular, isolated Zn atoms or highly dispersed ZnO nanoclusters have demonstrated to present high propene selectivity and catalytic stability in PDH system [17]. Schweitzer et al. observed high propene selectivity for single-site $Zn^{2+}$ on $SiO_2$, and pointed out that 3-coordinated $Zn^{2+}$ Lewis acid sites and coordinated environment of metal oxides was of great significance to design efficient metal oxide catalysts for PDH [18]. Shi et al. found that ZnO nanoparticle with an appropriate size of approximately 4.8 nm on $ZnO/SiO_2$ exhibited the maximum PDH activity and proposed that unsaturated $Zn^{2+}$ accompanied by oxygen vacancies were the active sites for the activation of C–H bond in propane [16]. However, ZnO-based material has its inherent stability defect due to the production of low-melting metallic Zn (420 $^{o}$C) under PDH reaction process. Also, some acidic supports such as molecular sieve may lead to low propene selectivity and poor stability of Zn-based catalyst due to side reactions and coking [19]. To overcome these shortcomings, constructing strong coordination interactions between active Zn species and the support with basicity, such as N-doped carbon material (N-C), is a feasible strategy. The notable examples are the design of highly dispersed Zn-based catalysts supported on N-C material from zeolitic imidazolate framework-8 [20, 21]. Owing to the stabilizing effect of the N-C material on ZnO nanoparticles, the catalysts showed high activity and stability for PDH reaction. However, the nature of the catalytically active Zn sites in Zn-based N-C material is still a matter of dispute.

Polyamide-imide (PAI), as an important, well-established and commercialized class of polymers prepared by the condensation of an aromatic diamine and an anhydride, can be good source for synthesis of the N-C material, which has strong anchoring effect for metal species and favorable surface modification [22, 23]. However, little is known about the utilization of PAI as the precursor to prepare Zn-based N-C material for PDH reaction. In this work, we develop a facile vacuum curing-carbonization approach to prepare a series of ZnO doped N-C material (ZnO-N-C) with small ZnO nanoparticles by using PAI as N-C source, zinc nitrate as metal source. The relationship between catalyst structure and the activity of Zn species in PDH reaction are explored by using a series of characterization techniques. Moreover, the probable active sites and deactivation factors for PDH reaction on the catalysts are proposed.

## 2. Experimental Section

### *2.1. Catalyst Preparation*

The series of xZnO-N-C catalysts (x stands for the weight percent of ZnO in the catalyst precursor) was prepared with a vacuum curing-carbonization process. Take 20ZnO-N-C as an example, the specific synthetic process was as follows. 4.00 g PAI (SR3602-37W, US cymer, solid content 38%, viscosity 5000 cps) was firstly dissolved in 30 mL N,N-dimethylformamide (DMF, Sinopharm Chemical Reagent Co., Ltd, China). And then 3.66 g $Zn(NO_3)_2{\cdot}6H_2O$ (Sinopharm Chemical Reagent Co., Ltd, China) and 1.00 g hexamethylenetetramine (Sinopharm Chemical Reagent Co., Ltd, China) were added to obtain the homogenous solution. The above-mentioned solution was then stirred at 150 $^{o}$C to form a viscous solid and further cured in vacuum at 150 $^{o}$C for 4 h to obtain the catalyst precursor. Finally, the precursor was carbonized at 500 $^{o}$C for 2 h then 600 $^{o}$C for 6 h in $N_2$ atmosphere at a ramping rate of 1.5 $^{o}$C·min$^{-1}$ to obtain the catalyst. The xZnO-N-C catalysts with ZnO weight percent of 5-40% were prepared by the process mentioned above by varying the adding amount of PAI and $Zn(NO_3)_2{\cdot}6H_2O$, respectively.

As a comparison, 20ZnO-N-C-air was prepared with the similar process above except that the obtained homogenous solution containing the same amount of PAI and $Zn(NO_3)_2{\cdot}6H_2O$ in DMF was cured at 240 $^{o}$C for 3 h in atmospheric air in order to obtain the material with less nitrogen-based species. Moreover, N-C material with only adding PAI, and ZnO material without adding PAI were also prepared by the same process mentioned above.

 doi:10.20944/preprints202311.1776.v1



*2.2. Catalytic Evaluation*

The direct dehydrogenation of propane to propene was carried out in a continuous flow quartz reaction tube at atmospheric pressure, packed by 0.50 g catalyst sample supported on 1.0 g quartz sand (60-80 mesh) and placed in the constant temperature zone of the reaction furnace. Propane gas (flowing rate 5.0-10.0 mL·min$^{-1}$ for 600-1200 h$^{-1}$ GHSV) was switched into the reactor after the reaction temperature reached the set value in $N_2$ flow (20 mL·min$^{-1}$). The outlet gas was analyzed by an on-line gas chromatography (GC2014, SHIMADZU) equipped with a hydrogen flame ionization detector packed with HP-AL/S capillary chromatographic column and a thermal conductivity detector provided with TDX-01 packed column, with sampling interval of 20 min. The carbon balance for all reactions was stabilized within the range of 100 ± 4%. Moreover, the deactivation rate constant ($k_d$, h$^{-1}$) of the catalyst was calculated by the following formula: $k_d = (\ln((1-X_{final})/X_{final}) - \ln((1-X_{initial})/X_{initial}))/t$, where $X_{initial}$ and $X_{final}$ represent the conversion of propane on the catalyst before and after reaction (%), $t$ stands for the reaction time (h).

*2.3. Catalyst Characterizations*

X-ray diffraction (XRD) of the samples was recorded by an X' Pert Pro multipurpose diffractometer (Smartlab-SE, Rigaku Corporation) with Cu K$\alpha$ radiation ($\lambda$ = 0.15418 nm) from 5° to 80° at room temperature.

Raman spectra of the catalysts were collected on a LabRam HR Evolution (HORIBA) equipped with a CCD detector and laser excitation ($\lambda$ = 532 nm) from 100 cm$^{-1}$ to 2500 cm$^{-1}$.

Transmission electron microscopy (TEM) and high-resolution transmission electron microscopy (HRTEM) of the catalysts were tested on Transmission Electron Microscope (TECNAI G$^2$ F20, FEI, US) instrument at 200 kV.

Fourier transform infrared spectroscopy (FTIR) of the catalysts was operated at wavenumbers from 4000 to 500 cm$^{-1}$ on a Nicolet Nexus 870 instrument.

X-ray photoelectron spectroscopy (XPS) analyses of the catalysts were performed on a Thermo Fisher Scientific K-Alpha spectrometer. The binding energy (BE) of the elements in the samples was referred to C 1s peak (284.8 eV).

$NH_3$ and $CO_2$ temperature-programmed desorption of the catalysts ($NH_3$-TPD and $CO_2$-TPD) were undertaken on ChemBET Pulsar TPR/TPD analyzer. Before the test, 50 mg of catalyst was pretreated to remove the adsorbed impurity at 400 °C for 60 min in He flow, followed by cooling to 100 °C and switching to adsorb $NH_3$ or $CO_2$ for 60 min. After cooling to room temperature in He flow, $NH_3$ or $CO_2$ desorption was carried out under He gas at a ramping rate of 10 °C·min$^{-1}$ to 900 °C.

Thermogravimetric measurements (TG) of the catalyst were determined on a NETZSCH STA 449F3 thermogravimetric analyzer from room temperature to 800 °C at a ramping rate of 10 °C·min$^{-1}$ in air.

## 3. Results and Discussion

*3.1. The Phase Structure and Nanoparticle Size of the Catalyst*

The phase structure of each catalyst is firstly characterized by XRD analysis, as shown in **Figure 1**. Obviously, the sharp and strong peaks in the pattern of ZnO catalyst, locate at 2$\theta$ positions of 31.8°, 34.4°, 36.2°, 47.5°, 56.6°, 62.9°, 66.4°, 68.0°, 69.1°, 72.6° and 77.0°, respectively correspond to the characteristic planes (100), (002), (101), (102), (110), (103), (200), (112), (201), (004) and (202) of ZnO hexagonal phase (JCPDS No. 36-1451) [24]. Meanwhile, the broad diffraction peak appeared at 22.4° is observed in the pattern of N-C based materials, demonstrating the amorphous carbon skeleton of the support [25]. Moreover, there is another weak and broad peak at 44.1 °, attributing to the (100) reflection plane of graphitized carbon [26, 27]. This means that N-C based catalysts are in certain degree of graphitization, consistent with the following Raman results. There is no signal about ZnO phase over 5ZnO-N-C, indicating its high dispersion on the catalyst. Further increasing the loading amount of ZnO to 10%, by sharp comparison, the featured diffraction peaks of ZnO with high

intensity appear. After careful calculation by Debye-Scherer equation, the grain size of ZnO for 10ZnO-N-C is 29.5 nm. However, further increasing ZnO content to 20-40%, the diffraction peaks attributed to ZnO grow weak and broad, suggesting the higher dispersion of ZnO nanoparticles on the catalysts. The grain sizes of ZnO are located at 5.1-7.4 nm on the 20-40ZnO-N-C catalysts, much smaller than that of 10ZnO-N-C. Notably, there is an exceptional case that the characteristic peaks belonged to ZnO in the XRD pattern of 10ZnO-N-C is obviously sharper than the other catalysts with higher ZnO content. It was carefully observed that much more foams could generate during the curing process of 10ZnO-N-C compared with other catalysts with different ZnO content, which indicated that the violent reaction easily caused the zinc enrichment on the catalyst surface, resulting in the agglomeration of ZnO species, which is further observed by the following TEM images. By comparison, the pure ZnO catalyst exhibits very larger grain size of ZnO with 62.4 nm, suggesting that loading ZnO onto the N-C material could severely reduce its grain size, thus improve its dispersion. Moreover, after carefully comparing the XRD diffraction peaks of 20ZnO-N-C and 20ZnO-N-C-air, as expected, the grain size of ZnO on 20ZnO-N-C-air (12.9 nm) is larger than twice that on 20ZnO-N-C (5.1 nm), suggesting the higher dispersion of ZnO nanoparticles on the latter.

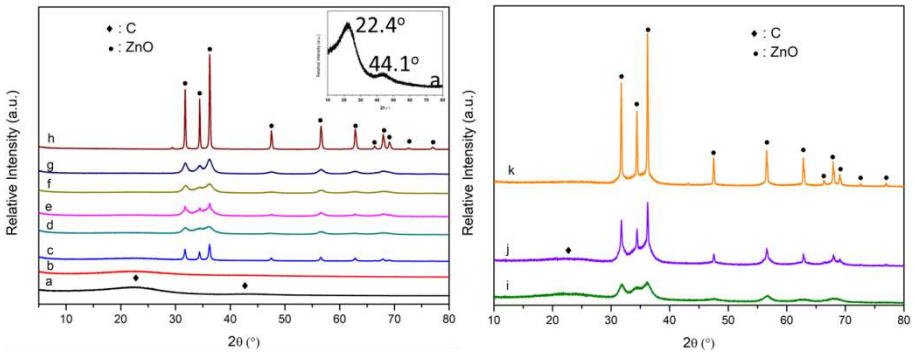


**Figure 1.** XRD patterns of the fresh catalysts (a) N-C; (b) 5ZnO-N-C; (c) 10ZnO-N-C; (d) 20ZnO-N-C; (e) 20ZnO-N-C-air; (f) 30ZnO-N-C; (g) 40ZnO-N-C; (h) ZnO and the spent catalysts (i) 20ZnO-N-C (GHSV = 840 $h^{-1}$, $T$ = 600 °C, $t$ = 2.5 h); (j) 20ZnO-N-C (GHSV = 840 $h^{-1}$, $T$ = 580 °C, $t$ = 6 h); (k) 20ZnO-N-C-air (GHSV = 840 $h^{-1}$, $T$ = 600 °C, $t$ = 2.5 h).

To determine the nanoparticle size and state of ZnO on the catalysts, TEM and HRTEM images are pictured in **Figure 2**. A large bulk structure with a smooth surface is observed on the N-C catalyst/support. Expectedly, no ZnO nanoparticles could be observed for the 5ZnO-N-C catalyst because of its high dispersion on the catalyst, very consistent with the XRD result. However, there are many accumulated ZnO nanoparticles with extremely heterogeneous distribution on the carbon support for 10ZnO-N-C. By statistics, the average size of ZnO nanoparticles is 35.9 nm. With the ZnO content further increasing to 20-40%, it can be observed that ZnO nanoparticles are highly dispersed on the catalyst. And its nanoparticle size is 5.5 nm, 6.8 nm and 8.2 nm for 20ZnO-N-C, 30ZnO-N-C and 40ZnO-N-C, respectively. By comparison with 20ZnO-N-C, 20ZnO-N-C-air exhibits the larger ZnO nanoparticle size of 13.8 nm, demonstrating the higher dispersion of ZnO nanoparticles over 20ZnO-N-C. However, the series above-mentioned catalysts show much smaller nanoparticle size than the pure ZnO catalyst (221.0 nm), suggesting that loading ZnO onto the N-C support could significantly hinder the growth of ZnO nanoparticles, also presenting the stabilization effect of the N-C material [20]. Moreover, HRTEM observations of the catalysts show that there are two exposed crystalline planes with an interplanar spacing of 0.284 nm and 0.264 nm, belonged to the characteristic ZnO (100) and ZnO (002) planes, respectively [28, 29].

Preprints (www.preprints.org) | NOT PEER-REVIEWED | Posted: 29 November 2023 doi:10.20944/preprints202311.1776.v1



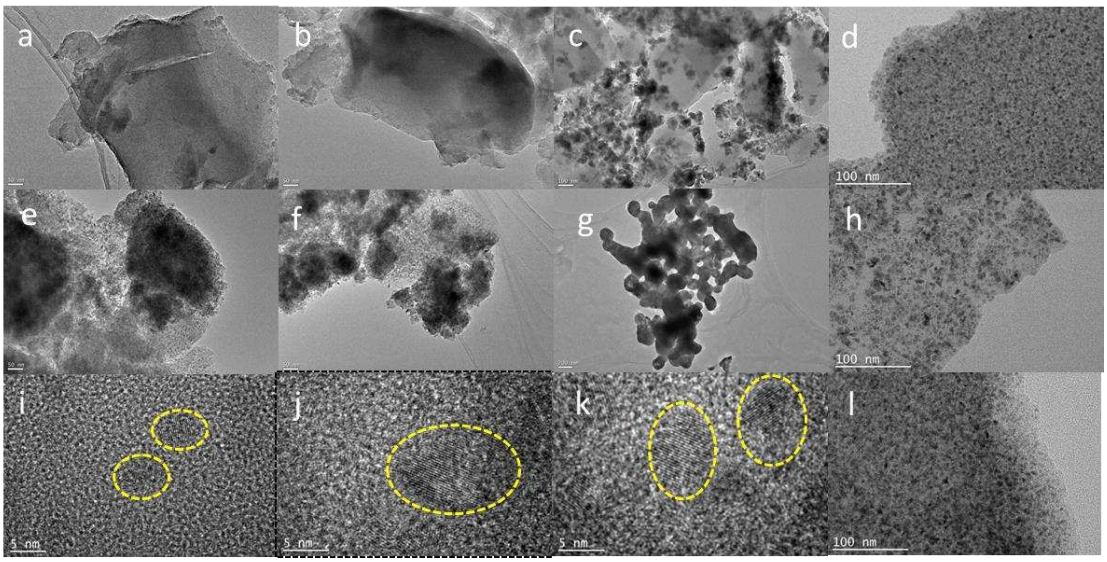


**Figure 2.** TEM images of (a) N-C; (b) 5ZnO-N-C; (c) 10ZnO-N-C; (d) 20ZnO-N-C; (e) 30ZnO-N-C; (f) 40ZnO-N-C; (g) ZnO; (h) 20ZnO-N-C-air; (l) the spent 20ZnO-N-C catalyst (GHSV = 840 $h^{-1}$, $T$ = 580 °C, $t$ = 6 h); The HRTEM images of (i) 20ZnO-N-C; (j) 20ZnO-N-C-air; (k) the spent 20ZnO-N-C catalyst (GHSV = 840 $h^{-1}$, $T$ = 580 °C, $t$ = 6 h).

The Raman spectra of the catalysts are further carried out and described in **Figure 3**. Apparently, no characteristic Raman bands of ZnO between 200 $cm^{-1}$ and 600 $cm^{-1}$ are observed on the catalysts [30]. However, all the catalysts exhibit the featured D-band and G-band at 1345 $cm^{-1}$ and 1590 $cm^{-1}$, which are attributed to the structural defect of carbon atomic lattice and stretching vibration of carbon atom $sp^2$ hybridization in plane [31, 32]. The $I_D/I_G$ value for Raman spectra is usually utilized to evaluate the graphitization of the carbon-based materials, as listed in **Figure 3**. By comparison with N-C, noticeably, the introduction of ZnO causes the $I_D/I_G$ value slightly increasing from 1.48 to 1.61-1.70, suggesting that ZnO may destroy the order of carbon materials, thus resulting in the reduction of graphitization degree of the carbon-based catalysts. With the further increase of ZnO content in the catalyst, the value of $I_D/I_G$ changes little, indicating that adjusting ZnO content could not take significant effect on the graphitization of carbon materials.

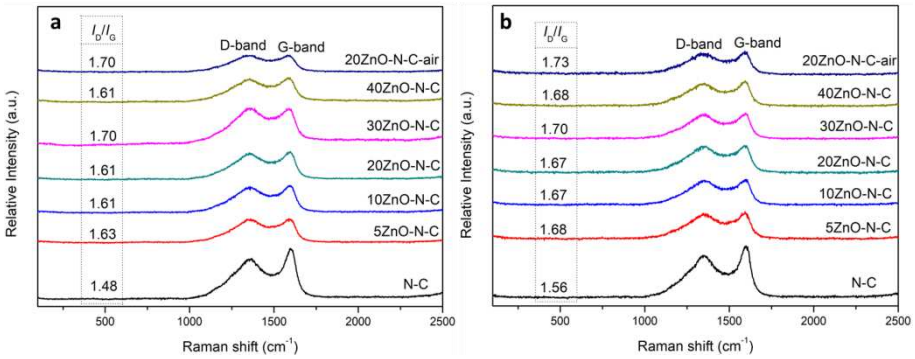


**Figure 3.** Raman spectra of (a) the fresh and (b) spent catalysts (GHSV = 840 $h^{-1}$, $T$ = 580 °C, $t$ = 6 h).

Preprints (www.preprints.org) | NOT PEER-REVIEWED | Posted: 29 November 2023 doi:10.20944/preprints202311.1776.v1



*3.2. The Surface Composition and State of the Catalyst*

FTIR spectra are conducted on recognizing the type of functional groups on the catalysts, as depicted in **Figure 4**. The observation shows that all catalysts with different ZnO contents display similarly shaped curves. The vibration of O-H at the wavenumber of 3432 $cm^{-1}$ is observed, indicating the presence of $H_2O$ molecules on the catalyst surface [33]. The stretching vibrations located at about 2810–3010 $cm^{-1}$ correspond to C-H bond [31]. The peaks at 1580 $cm^{-1}$ and 1280 $cm^{-1}$ can be attributed to C=N bond and N-H bond [34], indicating that N-containing species is successfully retained in the catalyst. Intensive bands around 1726 $cm^{-1}$ belong to the stretching

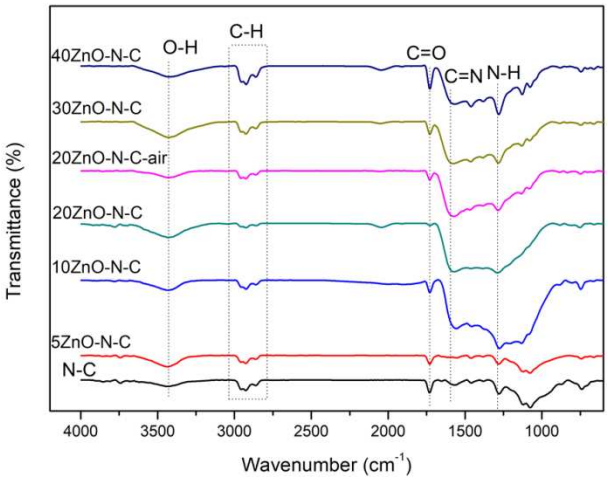


**Figure 4.** FTIR spectra of the fresh catalysts.

vibrations of C=O group, which is usually considered to be the active site of PDH on the carbon-based materials [35, 36]. However, the intensity of C=O bond in the spectra of 20ZnO-N-C is the weakest among all the catalysts, indicating that C=O species may not be the sole active site in the catalyst system for PDH reaction.

Furthermore, XPS spectra of the catalysts, shown in **Figure 5**, are carried out to detect the elemental composition and chemical state of the species on the catalyst surface. The spectra reveals the presence of Zn, N, O and C on xZnO-N-C catalyst surface, demonstrating that Zn species was successfully loaded and N species was maintained in the materials. The two peaks located at 1021.6-1022.3 eV and 1044.8-1045.5 eV are assigned to the $2p_{3/2}$ and $2p_{1/2}$ electronic states of $Zn^{2+}$, respectively [24]. Obviously, the binding energy of Zn 2p for ZnO obviously shift to higher direction in the xZnO-N-C and 20ZnO-N-C-air catalysts, indicating that the interaction between Zn species and N-C support such as Zn-$N_x$ coordination bond is formed during the preparation process. Moreover, the intensity of Zn 2p spectra becomes stronger for the xZnO-N-C catalyst with increasing ZnO content, demonstrating that the Zn content on the catalyst surface exhibit an increase momentum, as listed in **Table 1**. N 1s spectra of N-C could be clearly split into three peaks at 398.6 eV, 400.6 eV and 401.5 eV, which are associated with pyridinic-N, pyrrolic-N and graphitic-N species, respectively [37]. However, the deconvoluted N 1s spectra of the xZnO-N-C and 20ZNO-N-C-air reveal that another type of nitrogen-based species Zn-$N_x$, located at 399.4 eV, was present [15]. Therefore, the results confirm that Zn-$N_x$ species is formed in the carbon skeleton of xZnO-N-C. Moreover, 20ZnO-N-C exhibits the larger total amount of three nitrogen-based species (5.71%) and surface Zn-$N_x$ species (1.14%) than 20ZnO-N-C-air, which may result from the more thorough condensation reaction under vacuum compared in air. The O 1s signals of the catalysts exhibit three distinct peaks: lattice O ($O_{latt}$ : 530.4-530.7 eV) or Zn-O from ZnO, defect O ($O_{def}$ : 532.0-532.3 eV) or the O species of C=O group on the N-C support and adsorb O ($O_{ad}$ : 533.4-533.7 eV) or adsorbed $H_2O$ molecules [38]. As calculated in **Table 1**, 20ZnO-N-C possesses less content of the surface O species attributed to C=O group than 20ZnO-N-C-air, suggesting that C=O group is not the only active site for PDH reaction, consistent with the FTIR results.

Preprints (www.preprints.org) | NOT PEER-REVIEWED | Posted: 29 November 2023 doi:10.20944/preprints202311.1776.v1



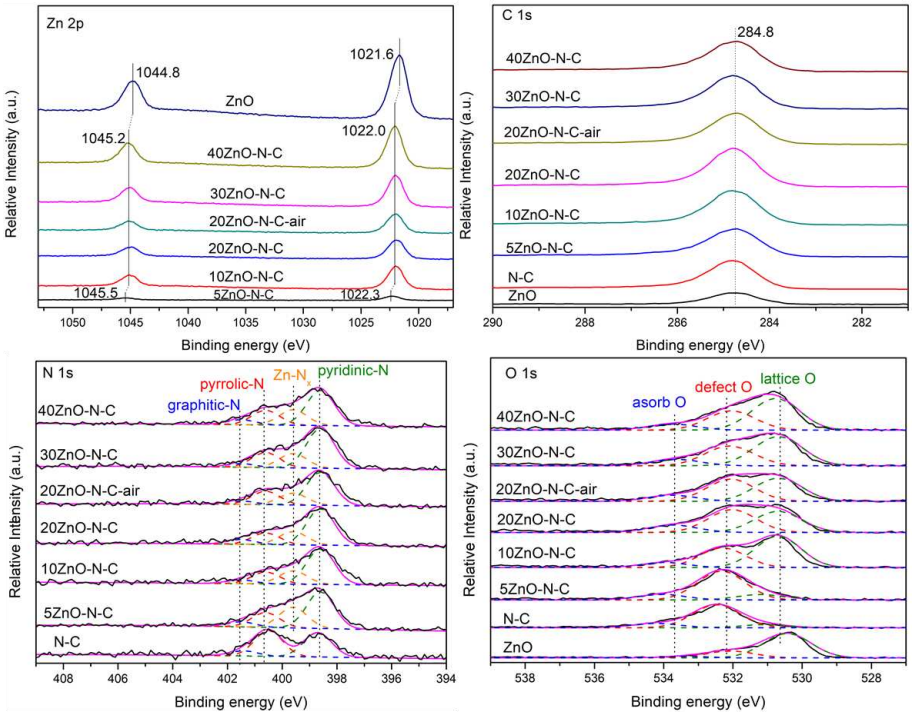


**Figure 5.** XPS spectra of the fresh catalysts.

**Table 1.** The contents of surface species on the fresh catalysts based on the XPS results.

| Catalyst | Atomic content (%) | | | | | | | | |
|---|---|---|---|---|---|---|---|---|---|
| | Zn | N | | | | O | | | C |
| | | Pyridinic-N | Zn-$N_x$ | Pyrrole-N | Graphitic-N | Zn-O | C=O | O-H | |
| N-C | 0 | 1.62 | 0 | 1.72 | 0.34 | 0 | 6.96 | 2.02 | 87.36 |
| 5ZnO-N-C | 1.46 | 3.44 | 1.95 | 1.39 | 0.48 | 1.29 | 6.02 | 1.25 | 82.73 |
| 10ZnO-N-C | 6.52 | 2.77 | 1.04 | 0.93 | 0.29 | 5.37 | 3.78 | 1.09 | 78.20 |
| 20ZnO-N-C | 5.26 | 3.16 | 1.14 | 1.02 | 0.40 | 4.32 | 4.20 | 1.02 | 79.49 |
| 30ZnO-N-C | 8.48 | 3.30 | 1.19 | 1.25 | 0.30 | 6.63 | 4.86 | 1.22 | 72.76 |
| 40ZnO-N-C | 10.73 | 3.04 | 1.34 | 1.26 | 0.43 | 8.20 | 4.66 | 1.33 | 69.02 |
| 20ZnO-N-C-air | 6.27 | 2.45 | 0.88 | 0.99 | 0.25 | 5.53 | 5.39 | 1.58 | 76.68 |

*3.3. The Acidity and Basicity of the Catalysts*

The acidity and basicity of the catalysts are important factors influencing the dehydrogenation activity and product selectivity [39]. Therefore, $NH_3$-TPD and $CO_2$-TPD characterizations are performed for each catalyst in order to detect the acidity and basicity of the catalysts, and the corresponding profiles are displayed in **Figure 6**. The peaks with weak intensities, located at 100-350 $^oC$ on the $NH_3$-TPD and $CO_2$-TPD profiles of the xZnO-N-C and 20ZnO-N-C-air catalysts, suggest the presence of tiny amount of acidity and basicity [40]. Obviously, both ZnO and N-C materials are hardly acidic or basic. After ZnO loading, the materials exhibit increasing amount of acidity and basicity, demonstrating that there are some interactions between Zn and N-C species, as proved by Raman and XPS characterizations. Moreover, the acidity and basicity of xZnO-N-C is different with the variation of ZnO loading, suggesting that the Zn loading amount can be utilized to adjust the acid sites and basic sites of the N-C based materials.

Preprints (www.preprints.org) | NOT PEER-REVIEWED | Posted: 29 November 2023 doi:10.20944/preprints202311.1776.v1



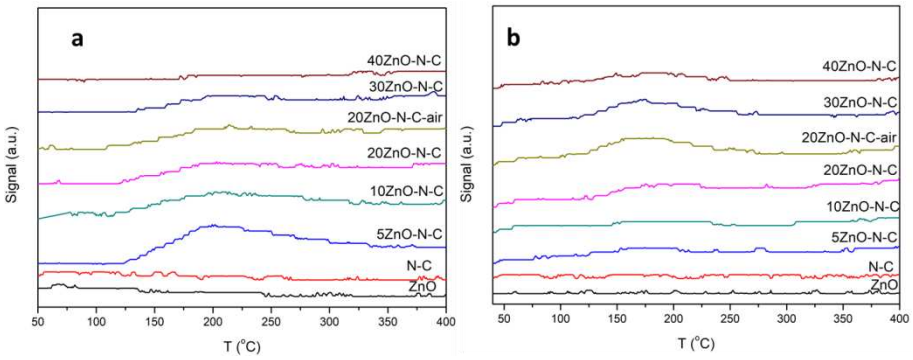


**Figure 6.** (a) $NH_3$-TPD and (b) $CO_2$-TPD profiles of the fresh catalysts.

*3.4. Catalytic Performance and Stability for PDH*

The catalytic performance of the above-mentioned materials in PDH reaction is firstly investigated, and the results are illustrated in **Figure 7**. Both ZnO and N-C catalyst presents propane conversion of about 20.0%, indicating that ZnO species and C=O species are both active sites for PDH reaction [17, 41]. By comparison, N-C material exhibits a little higher propene selectivity (46.5%) than ZnO catalyst. For the 20ZnO-N-C-air catalyst, the propane conversion and propylene selectivity both increase to 32.1% and 53.4%, which may be due to the co-elevation of acidity and basicity of the catalyst caused by the formation of Zn-$N_x$ coordination bond and the presence of electron-donating function groups such as nitrogen-based species. Sharply contrast, however, the 20ZnO-N-C catalyst presents advantages in product selectivity and catalytic stability. In specific, the higher propene selectivity (70.0%) with the propane conversion (35.2%) is obtained, suggesting that much more electron-donating function groups on 20ZnO-N-C favor the electron-rich product of propene to easily desorb from the catalyst surface, thus improving the product selectivity. In case of the catalytic stability, 20ZnO-N-C has the smaller deactivation rate constant ($k_d$ = 0.10 $h^{-1}$) than 20ZnO-N-C-air ($k_d$ = 0.38 $h^{-1}$), demonstrating the higher stability of the former, and the formation of Zn-$N_x$ strong coordination bond is conducive to the improvement of catalytic stability. Moreover, the propene selectivity gradually go up thus the propene yield reaches the maximum (27.3%) after 60 min reaction, then gradually decreases to 24.0% on the 20ZnO-N-C catalyst during 150 min reaction, similar to the initial propene yield (24.6%), also indicating the higher catalytic stability of the catalyst. By comparison, 20ZnO-N-C-air exhibits continuously decreasing propene yield from 17.1% to 10.0% during 150 min reaction. With the increment of ZnO loading, the propane conversion and propene selectivity both showed first increased and then decreased trend, demonstrating that the ZnO content of the catalyst could adjust the catalytic performance for PDH.

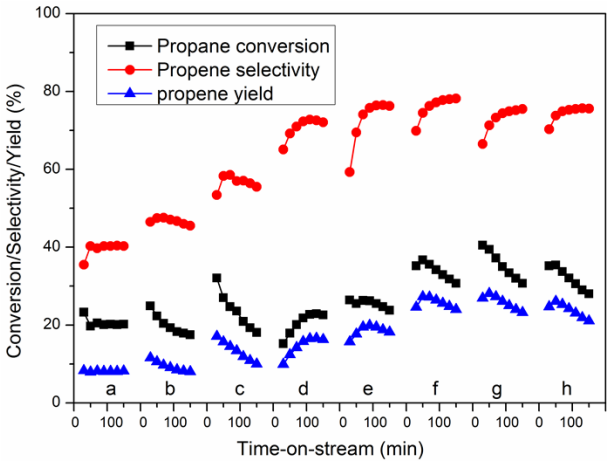


**Figure 7.** The catalytic performance of (a) ZnO; (b) N-C; (c) 20ZnO-N-C-air; (d) 5ZnO-N-C; (e) 10ZnO-N-C; (f) 20ZnO-N-C; (g) 30ZnO-N-C; (h) 40ZnO-N-C. Reaction conditions: GHSV = 840 $h^{-1}$, $T$ = 600 °C.

Preprints (www.preprints.org) | NOT PEER-REVIEWED | Posted: 29 November 2023 doi:10.20944/preprints202311.1776.v1



Then the influence of reaction temperature (T) and gas hourly space velocity (GHSV) of propane for the 20ZnO-N-C catalyst are carried out on PDH reaction, as shown in **Figure 8**. As expected, propane conversion greatly raises and propene selectivity of the catalyst gradually reduces with the reaction temperature increasing from 560 °C to 620 °C based on the endothermic characteristic of PDH reaction. Moreover, the $k_d$ value of 20ZnO-N-C becomes bigger, illustrating the lower catalytic stability with the increasing reaction temperature. Also expectedly, propane conversion of the catalyst gradually decreases, and propene selectivity and the catalytic stability improve with the GHSV of propane increasing from 600 $h^{-1}$ to 1200 $h^{-1}$. This is on account that the reduction in the contact time could avoid the occurrence of side reaction, therefore benefiting the propylene selectivity thus the catalytic stability.

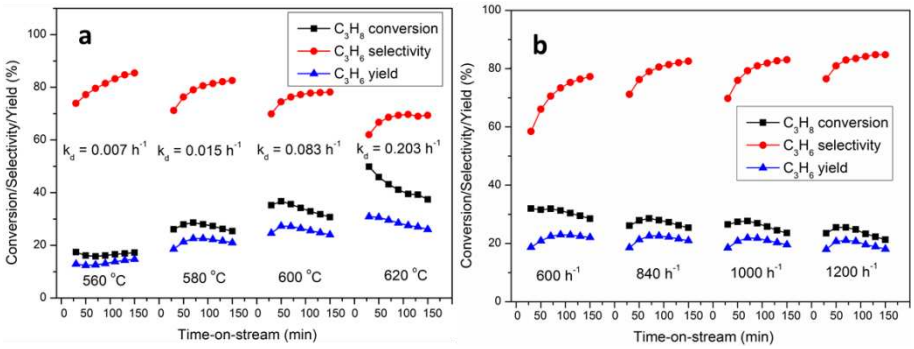


**Figure 8.** The catalytic performance of 20ZnO-N-C at (a) different temperatures with the same GHSV = 840 $h^{-1}$ and (B) different GHSVs with the same temperature $T$ = 580°C.

Finally, the catalytic stability of the 20ZnO-N-C catalyst at reaction temperature of 580 °C and GHSV of 840 $h^{-1}$ are performed for 6 h, as presented in Figure 9. The initial propane conversion and propene selectivity is 24.6% and 68.6% on the catalyst, respectively. With the increase of the time-on-stream, propane conversion shows a slightly decreased trend with a very small $k_d$ value of 0.071 $h^{-1}$. Nevertheless, the propene selectivity presents ascending trend and reaches 83.0% after reaction for about 150 min then remains, demonstrating that the high stability of the 20ZnO-N-C catalyst at the reaction condition of T = 580 °C and GHSV = 840 $h^{-1}$.

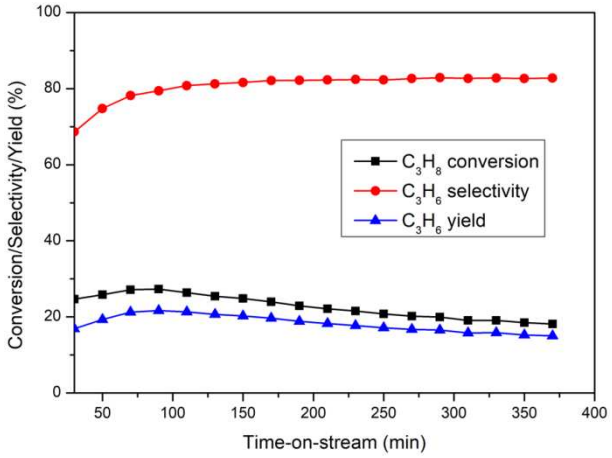


**Figure 9.** The catalytic performance of 20ZnO-N-C at GHSV = 840 $h^{-1}$, $T$ = 580°C.

*3.5. The Deactivation of the Catalyst*

It is well-known that the deactivation of the PDH catalyst could be caused by the coke formation and aggregation of the active nanoparticles on the catalyst [4, 42]. As a consequence, Raman spectra of the spent catalysts after reaction for 150 min are collected, as shown in Figure 3. It is observed that the $I_D/I_G$ value slightly increased from 1.48-1.70 of the fresh catalyst to 1.56-1.73 of the spent catalyst,

Preprints (www.preprints.org) | NOT PEER-REVIEWED | Posted: 29 November 2023 doi:10.20944/preprints202311.1776.v1



demonstrating the coke formation on the spent catalysts. Moreover, the deposited carbon may be mainly amorphous.

In order to investigate the coke amount on the spent catalysts, the TG curves of the fresh and spent N-C, 20ZnO-N-C-air and 20ZnO-N-C ($T$ = 600 °C, GHSV = 840 $h^{-1}$, $t$ = 150 min) are recorded, as shown in **Figure 10**. The coke amount is calculated using the weight loss between 300 °C and 700 °C. The amount of the deposited carbon for the N-C catalyst is 8.2 wt%. The 20ZnO-N-C-air catalyst possesses deposited carbon amount of 10.3 wt%. It was marvel to find that the 20ZnO-N-C catalyst exhibited slightly more coke accumulation (12.6 wt%) than 20ZnO-N-C-air. Combination with the catalytic performance, the coke formation is indeed one of the factors that resulted in the activity decrease, but it is probably not the main factor on the ZnO-N-C catalyst during the reaction.

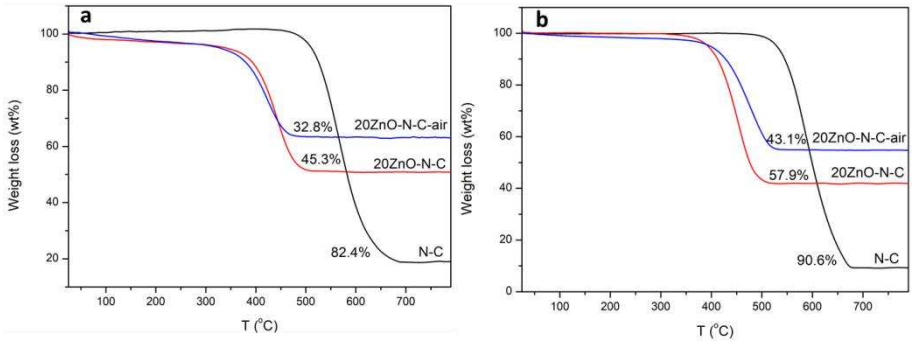


**Figure 10.** The TG curves of the (a) fresh and (b) spent catalysts at GHSV = 840 $h^{-1}$, $T$ = 600 °C, $t$ = 2.5 h.

In order to investigate the information about the nanoparticle size of ZnO, the XRD patterns of some representative spent catalysts are recorded, as presented in **Figure 1**. Obviously, the peak intensities belonged to ZnO phase in XRD pattern of the spent 20ZnO-N-C-air are significantly strengthened compared with those of the fresh catalyst. And ZnO grain size grows from 12.9 nm to 57.6 nm during the reaction, demonstrating the serious sintering of ZnO after reaction, which may be another cause for the activity loss. For 20ZnO-N-C, the characteristic peak intensity of ZnO do not change significantly after reaction, and the grain size of ZnO remain unchanged with about 5.0 nm. This phenomenon stated clearly that the 20ZnO-N-C catalyst possessed better anti-sintering ability than the 20ZnO-N-C-air catalyst. Moreover, the nanoparticle size of ZnO grew up from 5.5 nm on the fresh 20ZnO-N-C catalyst to 10.6 nm after 6 h reaction, as shown in TEM image (Figure 2), further demonstrating that the nanoparticle aggregation was the primary reason for the activity loss on the catalyst system.

## 4. Conclusions

In conclusion, the xZnO-N-C materials with small ZnO nanoparticles (5.5 nm) could be obtained with a facile vacuum curing-carbonization method using zinc nitrate as metal source and PAI as N-C source. Raman and XPS spectra suggest that much more nitrogen-based species especially Zn-$N_x$ coordination bond are formed on xZnO-N-C, thus leading to the co-elevation of the activity and basicity of the materials, as described in $NH_3$/$CO_2$-TPD profiles. Consequently, the 20ZnO-N-C samples exhibited much higher initial activity (propane conversion of 35.2% and propene yield of 24.6%) and relatively lower deactivation rate (0.071 $h^{-1}$) than 20ZnO-N-C-air prepared with curing-carbonization process in PDH reaction conducted at 600 °C. Based on the relationship of structure-activity, it is proposed that $Zn^{2+}$ species including Zn-$N_x$ and C=O on the N-C support are the probable active sites for PDH reaction. Furthermore, the aggregation of ZnO nanoparticles is the primary reason for the activity loss on this catalyst system based on XRD and TEM characterizations. The present finding provides a feasible construction strategy and valuable guidance for the design of efficient catalyst such as metal oxide doped nitrogen-carbon materials in dehydrogenation of light alkane.

**Author Contributions:** All authors reviewed the manuscript. Huahua Zhao contributed to conceptualization, experimental design and performance, writing and funding acquisition; Tingyu Ji contributed to data collection and formal analysis; Yanping Wu contributed to investigation and data curation; Huanling Song contributed to methodology and text editing. Jianfeng Wu contributed to funding acquisition, conceptualization and supervision; Lingjun Chou contributed to supervision and conceptualization.

**Data and code availability:** The raw/processed data is available to readers and can be accessed in an uploaded electronic repository.

**Acknowledgments:** The authors sincerely acknowledge the financial support from Lanzhou Institute of Chemical Physics (LICP) Cooperation Foundation for Young Scholars (HZJJ21-10), State Key Laboratory Program of Lanzhou Institute of Chemical Physics (LICP), Chinese Academy of Sciences (CHGZ-202209), National Natural Science Foundation of China (Nos. 21903041 and 21803027) and PetroChina Company Limited (LZSH-2022-JS-75).

**Conflicts of interest or competing interests:** The authors declare that they have no known competing financial interests or personal relationships that could have appeared to influence the work reported in this paper.

**Ethical approval:** This research does not include experiments involving human tissue and does not contain any studies with human participants or animals performed by any of the authors.

## References

1. van Koppen PAM, Bowers MT, Haynes CL, Armentrout PB (1998) Reactions of ground-state $Ti^+$ and $V^+$ with propane: Factors that govern C-H and C-C bond cleavage product branching ratios. J Am Chem Soc 120: 5704-5712. doi: 10.1021/ja974372s
2. Ali W, Prakash G, Maiti D (2021) Recent development in transition metal-catalysed C-H olefination. Chem Sci 12: 2735-2759. doi: 10.1039/d0sc05555g
3. Waku T, Biscardi JA, Iglesia E (2003) Active, selective, and stable Pt/Na-[Fe]ZSM5 catalyst for the dehydrogenation of light alkanes. Chem Commun: 1764-1765. doi:10.1039/b303506a
4. Zhang JS, Nakaya Y, Shimizu K, Furukawa S (2023) Surface engineering of titania boosts electroassisted propane dehydrogenation at low temperature. Angew Chem Int Ed. doi: 10.1002/anie.202300744
5. Lu JL, Fu BS, Kung MC, Xiao GM, Elam JW, Kung HH, Stair PC (2012) Coking- and sintering-resistant palladium catalysts achieved through atomic layer deposition. Science 335: 1205-1208. doi: 10.1126/science.1212906
6. Sattler JJHB, Ruiz-Martinez J, Santillan-Jimenez E, Weckhuysen BM (2014) Catalytic dehydrogenation of light alkanes on metals and metal oxides. Chem Rev 114: 10613-10653. doi: 10.1021/cr5002436
7. Sun YN, Wu YM, Tao L, Shan HH, Wang GW, Li CY (2015) Effect of pre-reduction on the performance of $Fe_2O_3/Al_2O_3$ catalysts in dehydrogenation of propane. J Mol Catal A Chem 397: 120-126. doi: 10.1016/j.molcata.2014.11.011
8. M Cheng, Zhao HH, Yang J, Zhao J, Yan L, Song HL, Chou LJ (2018) The catalytic dehydrogenation of isobutane and the stability enhancement over Fe incorporated SBA-15. Microporous Mesoporous Mater 266: 117-125. doi: 10.1016/j.micromeso.2018.02.046
9. Zhao ZJ, Wu TF, Xiong CY, Sun GD, Mu RT, Zeng L, Gong JL (2018) Hydroxyl-mediated non-oxidative propane dehydrogenation over $VO_x/\gamma$-$Al_2O_3$ catalysts with improved stability. Angew Chem Int Ed 57: 6791-6795. doi: 10.1002/anie.201800123
10. Cheng E, McCullough L, Noh H, Farha O, Hupp J, Notestein J (2020) Isobutane dehydrogenation over bulk and supported molybdenum sulfide catalysts. Ind Eng Chem Res 59: 1113-1122. doi: 10.1021/acs.iecr.9b05844
11. Han SL, Zhao D, Otroshchenko T, Lund H, Bentrup U, Kondratenko VA, Rockstroh N, Bartling S, Doronkin DE, Grunwaldt J, Rodemerck U, Linke D, Gao ML, Jiang GY, Kondratenko EV (2020) Elucidating the nature of active sites and fundamentals for their creation in Zn-containing $ZrO_2$-based catalysts for nonoxidative propane dehydrogenation. ACS Catal 10: 8933-8949. doi: 10.1021/acscatal.0c01580
12. Wang YS, Suo YJ, Ren JT, Wang Z, Yuan ZY (2021) Spatially isolated cobalt oxide sites derived from MOFs for direct propane dehydrogenation. J Colloid Interf Sci 594: 113-121. doi: 10.1016/j.jcis.2021.03.023
13. Liu G, Zeng L, Zhao ZJ, Tian H, Wu TF, Gong JL (2016) Platinum-modified $ZnO/Al_2O_3$ for propane dehydrogenation: minimized platinum usage and improved catalytic stability. ACS Catal 6: 2158-2162. doi: 10.1021/acscatal.5b02878
14. Cheng M, Zhao HH, Yang J, Zhao J, Yan L, Song HL, Chou LJ (2019) Facile synthesis of ordered mesoporous zinc alumina catalysts and their dehydrogenation behavior. RSC Adv 9: 9828-9837. doi: 10.1039/c9ra00217k

15. Li J, Chen SG, Yang N, Deng MM, Ibraheem S, Deng JH, Li J, Li L, Wei ZD (2019) Ultrahigh-loading zinc single-atom catalyst for highly efficient oxygen reduction in both acidic and alkaline media. Angew Chem Int Ed 58: 7035-7039. doi: 10.1002/anie.201902109
16. Shi XX, Chen S, Li S, Yang YQ, Guan QQ, Ding JN, Liu XY, Liu Q, Xu WL, Lu JL (2023) Particle size effect of $SiO_2$-supported ZnO catalysts in propane dehydrogenation. Catal Sci Technol 13: 1866-1873. doi: 10.1039/d2cy02131e
17. Yuan Y, Lobo RF (2023) Zinc speciation and propane dehydrogenation in Zn/H-ZSM-5 catalysts. ACS Catal 13: 4971-4984. doi: 10.1021/acscatal.2c05898
18. Schweitzer NM, Hu B, Das U, Kim H, Greeley J, Curtiss LA, Stair PC, Miller JT, Hock AS (2014) Propylene hydrogenation and propane dehydrogenation by a single-Site $Zn^{2+}$ on silica catalyst. ACS Catal 4: 1091-1098. doi: 10.1021/cs401116p
19. Almutairi SMT, Mezari B, Magusin PCMM, Pidko EA, Hensen EJM (2012) Structure and reactivity of Zn-modified ZSM-5 zeolites: The importance of clustered cationic Zn complexes. ACS Catal 2: 71-83. doi: 10.1021/cs200441e
20. D Zhao, YM Li, SL Han, YY Zhang, GY Jiang, YJ Wang, K Guo, Z Zhao, CM Xu, RJ Li, CC Yu, J Zhang, BH Ge, EV Kondratenko (2019) ZnO Nanoparticles encapsulated in nitrogen-doped carbon material and silicalite-1 composites for efficient propane dehydrogenation. iScience 13: 269-276. doi: 10.1016/j.isci.2019.02.018
21. Cao TL, Dai XY, Fu Y, Qi W (2023) Coordination polymer-derived non-precious metal catalyst for propane dehydrogenation: Highly dispersed zinc anchored on N-doped carbon. Appl Surf Sci 607: 155055. doi: 10.1016/j.apsusc.2022.155055
22. Feng QP, Xie XM, Liu YT, Zhao W, Gao YF (2007) Synthesis of hyperbranched aromatic polyamide-imide and its grafting onto multiwalled carbon nanotubes. J Appl Polym Sci 106: 2413-2421. doi: 10.1002/app.26772
23. Duan GG, Liu SW, Jiang SH, Hou HQ (2019) High-performance polyamide-imide films and electrospun aligned nanofibers from an amide-containing diamine. J Mater Sci 54: 6719-6727. doi: 10.1007/s10853-019-03326-w
24. Singh K, Nancy, Kaur H, Sharma PK, Singh G, Singh J (2023) ZnO and cobalt decorated ZnO NPs: Synthesis, photocatalysis and antimicrobial applications. Chemosphere 313: 137322. doi: 10.1016/j.chemosphere.2022.137322
25. Han JH, Johnson I, Lu Z, Kudo A, Chen MW (2021) Effect of local atomic structure on sodium ion storage in hard amorphous carbon. Nano Lett 21: 6504-6510. doi: 10.1021/acs.nanolett.1c01595
26. Z Liu, ZY Du, W Xing, ZF Yan (2014) Facial synthesis of N-doped microporous carbon derived from urea furfural resin with high $CO_2$ capture capacity. Mater Lett 117: 273-275. doi: 10.1016/j.matlet.2013.12.021
27. Cao PK, Liu YM, Quan X, Zhao JJ, Chen S, Yu HT (2019) Nitrogen-doped hierarchically porous carbon nanopolyhedras derived from core-shell ZIF-8@ZIF-8 single crystals for enhanced oxygen reduction reaction. Catal Today 327: 366-373. doi: 10.1016/j.cattod.2018.03.020
28. Wang LH, Han XD, Zhang YF, Zheng K, Liu P, Zhang Z (2011) Asymmetrical quantum dot growth on tensile and compressive-strained ZnO nanowire surfaces. Acta Mater 59: 651-657. doi: 10.1016/j.actamat.2010.10.001
29. Wong TI, Tan HR, Sentosa D, Wong LM, Wang SJ, Feng YP (2012) Epitaxial growth of ZnO film on Si(111) with $CeO_2$(111) as buffer layer. J Phys D Appl Phys 45: 415306. doi: 10.1088/0022-3727/45/41/415306
30. JG Yu, HZ Xing, QQ Zhao, HB Mao, Y Shen, JQ Wang, ZS Lai, ZQ Zhu (2006) The origin of additional modes in Raman spectra of $N^+$-implanted ZnO. Solid State Commun 138: 502-504. doi: 10.1016/j.ssc.2006.04.019
31. Zhao HH, Song HL, Zhao J, Yang J, Yan L, Chou LJ (2020) The Reactivity and deactivation mechanism of Ru@C catalyst over hydrogenation of aromatics to cyclohexane derivatives. Chemistryselect 5: 4316-4327. doi: 10.1002/slct.202000311
32. Liang MF, Liu Y, Zhang J, Wang FY, Miao ZC, Diao LC, Mu JL, Zhou J, Zhuo SP (2022) Understanding the role of metal and N species in M@NC catalysts for electrochemical $CO_2$ reduction reaction. Appl Catal B: Environ 306: 121115. doi: 10.1016/j.apcatb.2022.121115
33. Gunawan ER, Suhendra D, Hidayat I, Kurniawati L (2018) Optimization of alkyldiethanolamides synthesis from terminalia catappa L. kernel oil through enzymatic reaction, J Oleo Sci 67: 949-955. doi: 10.5650/jos.ess18042
34. Przepiórski J, Skrodzewicz M, Morawski AW (2004) High temperature ammonia treatment of activated carbon for enhancement of $CO_2$ adsorption. Appl Surf Sci 225: 235-242. doi: 10.1016/j.apsusc.2003.10.006
35. Qi W, Liu W, Zhang BS, Gu XM, Guo XL, Su DS (2013) Oxidative dehydrogenation on nanocarbon: Identification and quantification of active sites by chemical titration, Angew Chem Int Ed 52: 14224-14228. doi: 10.1002/anie.201306825
36. Sun XY, Li B, Su DS (2014) Revealing the nature of the active site on the carbon catalyst for C-H bond activation, Chem Commun 50: 11016-11019. doi: 10.1039/c4cc02841d

37. Zheng FC, Yang Y, Chen QW (2014) High lithium anodic performance of highly nitrogen-doped porous carbon prepared from a metal-organic framework. Nat Commun 5: 5261 doi: 10.1038/ncomms6261
38. QQ Guo, Jing W, Hou YQ, Huang ZG, M GQ a, Han XJ, Sun DK (2015) On the nature of oxygen groups for $NH_3$-SCR of NO over carbon at low temperatures. Chem Eng J 270: 41-49. doi: 10.1016/j.cej.2015.01.086
39. Ren YJ, Zhang F, Hua WM, Yue YH, Gao Z (2009) ZnO supported on high silica HZSM-5 as new catalysts for dehydrogenation of propane to propene in the presence of $CO_2$. Catal Today 148: 316-322. doi: 10.1016/j.cattod.2009.05.011
40. Zhao HH, Song HL, Chou LJ, Zhao J, Yang J, Yan L (2017) Insight into the structure and molybdenum species in mesoporous molybdena-alumina catalysts for isobutane dehydrogenation. Catal Sci Technol 7: 3258-3267. doi: 10.1039/c7cy00975e
41. Zhang J, Liu X, Blume R, Zhang AH, Schloegl R, Su DS (2008) Surface-modified carbon nanotubes catalyze oxidative dehydrogenation of n-butane. Science 322: 73-77. doi: 10.1126/science.1161916
42. Otroshchenko T, Jiang G, Kondratenko VA, Rodemerck U, Kondratenko EV (2021) Current status and perspectives in oxidative, non-oxidative and $CO_2$-mediated dehydrogenation of propane and isobutane over metal oxide catalysts. Chem Soc Rev 50: 473-527. doi: 10.1039/d0cs01140a